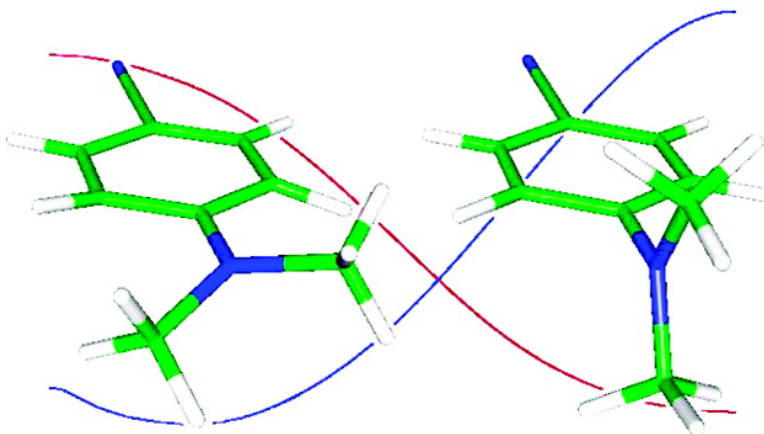


On the Nature of the Low-Lying Singlet States of 4-(Dimethyl-amino)benzonitrile

Andreas Khn, and Christof Httig

J. Am. Chem. Soc., **2004**, 126 (23), 7399-7410 • DOI: 10.1021/ja0490572 • Publication Date (Web): 25 May 2004

Downloaded from <http://pubs.acs.org> on March 31, 2009



More About This Article

Additional resources and features associated with this article are available within the HTML version:

- Supporting Information
- Links to the 3 articles that cite this article, as of the time of this article download
- Access to high resolution figures
- Links to articles and content related to this article
- Copyright permission to reproduce figures and/or text from this article

[View the Full Text HTML](#)



On the Nature of the Low-Lying Singlet States of 4-(Dimethyl-amino)benzonitrile

Andreas Köhn*[†] and Christof Hättig

Contribution from the Forschungszentrum Karlsruhe, Institute of Nanotechnology,
P.O. Box 3640, D-76021 Karlsruhe, Germany

Received February 19, 2004; E-mail: andreas@chem.au.dk

Abstract: 4-(*N,N*-Dimethyl-amino)benzonitrile (DMABN) is a prototype molecule for dual fluorescence. The anomalous emission has been attributed to an intramolecular charge-transfer (ICT) state, and the structure of the latter is still subject to some controversy. We applied a recently developed analytical gradient code for the approximate coupled-cluster singles-and-doubles method CC2 in combination with accurate basis sets to address this problem. Fully optimized excited state structures are presented for the ICT state and the so-called locally excited state, and recent transient IR and Raman measurements on the excited states are interpreted by means of calculated harmonic frequencies. Strong evidence is found for an electronic decoupling of the phenyl and the dimethyl-amino moiety, resulting in a minimum structure for the ICT state with a twisted geometry. In contrast to previous findings, the structure of this state is, at least in the gas phase, not C_{2v} symmetric but distorted towards C_s symmetry. The distortion coordinate is a pyramidalization of the phenyl carbon atom carrying the dimethyl-amino group. The results from the CC2 model are supported by single-point calculations using more elaborate coupled-cluster models (CCSD, CCSDR(3)) and by CASSCF calculations.

1. Introduction

4-(*N,N*-Dimethyl-amino)benzonitrile (DMABN) is probably the most prominent representative of a class of donor–acceptor substituted benzene derivatives with unusual fluorescence properties. More than 40 years ago, Lippert and co-workers¹ observed that in solutions of DMABN, apart from the expected fluorescence band, a second strongly red-shifted band appears which shows a marked dependence on solvent polarity and temperature. This phenomenon was termed “dual fluorescence”. The “normal” fluorescence band was assigned to a 1L_b -type state (B band), and the “anomalous” band was attributed to a 1L_a -type state which was expected to have a large dipole moment. Grabowski et al.^{2,3} suggested a mechanism that involved, in the electronically excited state, a charge transfer from the dimethyl-amino group to the benzonitrile moiety accompanied by a 90° twist of the dimethyl-amino group relative to the ring plane of the remaining π -system. The two subunits were assumed to be thus electronically decoupled (principle of minimum overlap⁴). This model was termed *twisted intramolecular charge transfer* (TICT). Later it was shown that the ICT state cannot be populated through direct absorption of a photon.⁵ Rather, first

the L_b -type state, also termed locally excited (LE) state, is populated which on a picosecond time scale can convert into the anomalously fluorescing state. Zachariasse et al. have also pointed out that a small energy gap (between the 1L_a and 1L_b states) in the Franck–Condon region is another important prerequisite for the occurrence of dual fluorescence.⁶ Above that, the assumption of electronic decoupling between the dimethyl-amino and the benzonitrile moiety was criticized,^{7,8} and an alternative reaction coordinate was put forward: the planarization of the dimethyl-amino group and a coupling of the nitrogen lone pair to the π -system in the sense of a quinoid electron system.^{7,8} For this model, the term “planar intramolecular charge transfer” (PICT) was coined.^{8,9} Further alternative reaction coordinates^{10–12} have been discussed too, but there is nowadays common agreement that these are not primarily involved in the ICT process.

Only recently, while the manuscript of this article was being revised, a new paper appeared¹³ in which the occurrence of ICT was reported for 1-*tert*-butyl-6-cyano-1,2,3,4-tetrahydroquinoline (NTC6), a “planarized” molecule in which the twisting motion is considered as sterically hindered. This has been taken as

[†] New address: Department of Chemistry, Århus University, DK-8000 Århus, Denmark.

- (1) Lippert, E.; Lüder, W.; Boos, H. In *Advances in Molecular Spectroscopy*; Mangini, A., Ed.; Pergamon: Oxford, 1962; pp 443–457.
- (2) Grabowski, Z. R.; Rotkiewicz, K.; Siemiarczuk, A.; Cowley, D. J.; Baumann, W. *Nouv. J. Chim.* **1979**, *3*, 443–454.
- (3) Rotkiewicz, K.; Grellmann, K. H.; Grabowski, Z. R. *Chem. Phys. Lett.* **1973**, *19*, 315–318.
- (4) Rettig, W. *Angew. Chem., Int. Ed.* **1986**, *25*, 971–988.
- (5) Leinhos, U.; Kühnle, W.; Zachariasse, K. A. *J. Phys. Chem.* **1991**, *95*, 2013–2021.

- (6) Zachariasse, K. A.; von der Haar, T.; Hebecker, A.; Leinhos, U.; Kühnle, W. *Pure Appl. Chem.* **1993**, *65*, 1745–1750.
- (7) von der Haar, T.; Hebecker, A.; Il'ichev, Y.; Jiang, Y.-B.; Kühnle, W.; Zachariasse, K. *Recl. Trav. Chim. Pays-Bas* **1995**, *114*, 430–442.
- (8) Il'ichev, Y. V.; Kühnle, W.; Zachariasse, K. A. *J. Phys. Chem. A* **1998**, *102*, 5670–5680.
- (9) Zachariasse, K. A. *Chem. Phys. Lett.* **2000**, *320*, 8–13.
- (10) Schuddeboom, W.; Jonker, S. A.; Warman, J. M.; Leinhos, U.; Kühnle, W.; Zachariasse, K. A. *J. Phys. Chem.* **1992**, *96*, 10809–10819.
- (11) Gorse, A.-D.; Pesquer, M. *J. Phys. Chem.* **1995**, *98*, 4039–4049.
- (12) Sobolewski, A. L.; Domcke, W. *Chem. Phys. Lett.* **1996**, *259*, 119–127.
- (13) Zachariasse, K.; Druzhinin, S.; Bosch, W.; Machinek, R. *J. Am. Chem. Soc.* **2004**, *126*, 1705–1715.

indication that the twisting motion is no necessary prerequisite for the formation of an ICT state in amino-benzonitriles. However, up to now not much is known about structures of molecules in electronically excited states, and it is not clear to what extent empirical rules for ground states can be readily transferred (see section 4 of this paper).

The ongoing debate on the various models has in recent decades stimulated many theoreticians to work on DMABN and related systems, and a long list of publications exists (e.g., refs 12, 14–26). The main motivation for employing quantum mechanical calculations for these systems lies in the large complexity of the problem, which cannot be solved based on simple qualitative models alone (see also the analogous comments in the conclusions of ref 26). The main task of theoretical work is therefore to augment the experimental work by (a) testing the employed models on consistency with quantum mechanical rules and (b) offering further predictions on which the models can be verified experimentally.

The long list of theoretical work mentioned above may indeed be confusing for nonexperts which are not in every detail aware of the strengths and weaknesses of the different methods, although most authors tried to point out the limitations of their work. Certainly, each of the above contributions added another important element to the puzzle, and in great detail all the studies converge to the same picture, viz. that only the twisting of the dimethyl-amino group leads to an low-lying ICT state. Yet, a detailed knowledge on the actual minimum structure of the ICT state is missing as discussed in the following.

In particular, due to the absence of efficient analytical gradient codes, no excited state geometry optimizations have so far been carried out at a level beyond configuration interaction in the space of single excitations (CIS) or complete active space self-consistent field (CASSCF); i.e., dynamic electron correlation has been neglected so far. Above that, only moderately sized basis sets of double- ζ quality were employed which additionally limited the accuracy. The need for relaxed excited-state structures, and analytical gradient codes is even more obvious for the interpretation of recent experimental results on the vibrational modes of the states involved in the ICT process.^{27–33} In particular, it was suggested^{21,34} to monitor the Ph-N vibration which was at the CASSCF level predicted to shift down for a TICT state and to shift up for a PICT state.²¹ Based on this prediction, Kwok et al.^{28,29} interpreted their time-resolved Raman

spectra in favor of the TICT hypothesis. The accuracy of the CASSCF calculations³⁵ and the direct relation between structure and vibrational normal modes, however, has been criticized by Okamoto et al.^{31,30}

Only in a very recent work, Rappoport and Furche²⁶ carried out full geometry optimizations of the excited states of DMABN employing time-dependent density functional theory (TDDFT) and large basis sets of triple- ζ valence quality. They also calculated the vibrational frequencies and gave a detailed interpretation of the spectra. However, the results presented in this study, in particular the reaction energies, are impaired by the problems that currently available functionals encounter for charge-transfer states (see, e.g., ref 36). For example, a much too large exothermic LE \rightarrow ICT reaction is predicted, as clearly stated by the authors.²⁶ Also, the energy curve of the LE state along the torsion coordinate shows an odd behavior, staying nearly constant with two minima at 32.5° and 90°. Certainly, the results of this study need to be augmented by more precise methods to obtain a more satisfactory picture of the ICT process.

In this communication, we present for the first time relaxed excited-state structures and vibrational frequencies obtained from a pure ab initio method that includes electron correlation, employing triple- ζ valence basis sets, and fully optimized structures for the excited states. The employed method stems from the coupled-cluster (CC) family of methods and treats electron correlation up to second-order perturbation theory. It has been termed CC2³⁷ and can be viewed as an approximation to the coupled-cluster singles and doubles (CCSD) model. We have recently developed an analytic gradient program^{38,39} for an improved CC2 code,⁴⁰ with respect to computation times, that made this extensive application feasible.

2. Computational Procedure

Ground and excited state structures were optimized at the ab initio level using the analytic RI-CC2 gradient code^{38–40} of the TURBOMOLE program package.⁴¹ CC2 compares with respect to both accuracy and computational effort with second-order Møller–Plesset perturbation theory (MP2) for the ground state. In contrast to the latter, it also allows for the calculation of excited-state energies. We note that the method relies on a predominant single-reference character of the *ground state*. The excited state should be dominated by single replacements with respect to the ground state wave function. The resolution-of-the-identity (RI) approximation^{42–44} is used to improve the efficiency of the code without sacrificing the accuracy of the results.^{39,40,45}

- (14) Serrano Andrés, L.; Merchán, M.; Roos, B. O.; Lindh, R. *J. Am. Chem. Soc.* **1995**, *117*, 3189–3204.
- (15) Sobolewski, A. L.; Sudholt, W.; Domcke, W. *J. Phys. Chem. A* **1998**, *102*, 2716–2722.
- (16) Sudholt, W.; Sobolewski, A. L.; Domcke, W. *Chem. Phys.* **1999**, *240*, 9–18.
- (17) Sudholt, W.; Staib, A.; Sobolewski, A. L.; Domcke, W. *Phys. Chem. Chem. Phys.* **2000**, *2*, 4341–4353.
- (18) Parusel, A. B. J.; Köhler, G.; Grimme, S. *J. Phys. Chem. A* **1998**, *102*, 6297–6306.
- (19) Parusel, A. B. J.; Köhler, G.; Nooijen, M. *J. Phys. Chem. A* **1999**, *103*, 4056–4064.
- (20) Parusel, A. B. J.; Rettig, W.; Sudholt, W. *J. Phys. Chem. A* **2002**, *106*, 804–815.
- (21) Dreyer, J.; Kummrow, A. *J. Am. Chem. Soc.* **2000**, *122*, 2577–2585.
- (22) Cammi, R.; Menucci, B.; Tomasi, J. *J. Phys. Chem. A* **2000**, *104*, 5631–5637.
- (23) Menucci, B.; Toniolo, A.; Tomasi, J. *J. Am. Chem. Soc.* **2000**, *122*, 10621–10630.
- (24) Zilberg, S.; Haas, Y. *J. Phys. Chem. A* **2002**, *106*, 1–11.
- (25) Jamorski Jödicke, C.; Lüthi, H. P. *J. Chem. Phys.* **2002**, *117*, 4146–4167.
- (26) Rappoport, D.; Furche, F. *J. Am. Chem. Soc.* **2004**, *126*, 1277–1284.
- (27) Hashimoto, M.; Hamaguchi, H. *J. Phys. Chem.* **1995**, *99*, 7875–7877.
- (28) Kwok, W. M.; Ma, C.; Matousek, P.; Parker, A. W.; Phillips, D.; Toner, W. T.; Towrie, M. *Chem. Phys. Lett.* **2000**, *322*, 395–400.
- (29) Kwok, W. M.; Ma, C.; Matousek, P.; Parker, A. W.; Phillips, D.; Toner, W. T.; Towrie, M.; Umapathy, S. *J. Phys. Chem. A* **2001**, *105*, 984–990.

- (30) Okamoto, H.; Inishi, H.; Nakamura, Y.; Kohtani, S.; Nakagaki, R. *J. Phys. Chem. A* **2001**, *105*, 4182–4188.
- (31) Okamoto, H.; Kinoshita, M.; Kohtani, S.; Nakagaki, R.; Zachariasse, K. A. *Bull. Chem. Soc. Jpn.* **2002**, *75*, 957–963.
- (32) Kwok, W. M.; Ma, C.; Phillips, D.; Matousek, P.; Parker, A. W.; Towrie, M. *J. Phys. Chem. A* **2000**, *104*, 4188–4197.
- (33) Ma, C.; Kwok, W. M.; Matousek, P.; Parker, A. W.; Phillips, D.; Toner, W. T.; Towrie, M. *J. Phys. Chem. A* **2002**, *106*, 3294–3305.
- (34) Chudoba, C.; Kummrow, A.; Dreyer, J.; Stenger, J.; Nibbering, E.; Elsaesser, T.; Zachariasse, K. *Chem. Phys. Lett.* **1999**, *309*, 357–363.
- (35) It should be noted, however, that the neglect of correlation effects causes CASSCF force constants (like CIS force constants) to be too high, especially if only very small active spaces are chosen. The authors of ref 21 therefore had to use the usual scaling factor for Hartree–Fock force-constant calculations of 0.9 to obtain results that can be compared to experimental numbers.
- (36) Tozer, D. J. *J. Chem. Phys.* **2003**, *119*, 12697–12699.
- (37) Christiansen, O.; Koch, H.; Jørgensen, P. *Chem. Phys. Lett.* **1995**, *243*, 409–418.
- (38) Hättig, C. *J. Chem. Phys.* **2003**, *118*, 7751–7761.
- (39) Köhn, A.; Hättig, C. *J. Chem. Phys.* **2003**, *119*, 5021–5036.
- (40) Hättig, C.; Weigend, F. *J. Chem. Phys.* **2000**, *113*, 5154–5162.
- (41) Ahlrichs, R.; Bär, M.; Horn, H.; Kölmel, C. *Chem. Phys. Lett.* **1989**, *162*, 165–169.
- (42) Whitten, J. L. *J. Chem. Phys.* **1973**, *58*, 4496–4501.
- (43) Dunlap, B. I.; Conolly, J. W. D.; Sabin, J. R. *J. Chem. Phys.* **1979**, *71*, 3396–3402.

Table 1. Structures, Dipole Moments, and Energy Separations Calculated for the States Considered in This Work in Comparison to Available Experimental Data

	ground state		LE state		ICT state		
	CC2/TZVPP	expt	CC2/TZVPP	expt	CC2/TZVPP	CC2/TZVPP	expt
	Structure ^a (Bond Lengths in pm, Angles in deg)						
point group	C _s		C ₂		C _{2v}	C _s	
NMe	145.0	143.9/145.6 ^b	145.2		145.2	144.5/145.5	
d(NC ₄)	137.7	136.5	138.8		142.0	144.3	
d(C ₃ C ₄)	141.4	140.0	141.6		143.0	144.6	
d(C ₂ C ₃)	138.7	137.0	143.6		137.3	137.2	
d(C ₁ C ₂)	140.2	138.8	141.3		143.8	142.9	
d(C ₁ C)	142.7	142.7	142.6		140.5	140.9	
d(CN)	118.2	114.5	118.3		119.2	118.9	
ω ^c	23	11.9	0		0	0	
τ ^d	0	0	19	26 ^e	90	90	
φ ^f	<1		0		0	41	
	Dipole moment (Debye)						
μ	7.4	6.6 ^g	10.1	9.7 ^h	15.1	13.3	16.1 ^h
	Energy Separations (eV)						
ΔE ⁱ			3.78	3.76 ^j	3.27	2.49	2.8/3.0/3.2 ^k
T _e ^l			4.14		4.16	4.06	
ν ₀₀ ^m			3.96	3.998 ⁿ	3.96	3.91	

^a For numbering of the atoms, see Figure 1. ^b X-ray data from ref 51. The two methyl groups were not considered equivalent. ^c “Wagging angle” of the dimethyl-amino group, defined as angle of a straight line given by the NC₄ bond with respect to a plane given by N and the carbon atoms of the methyl groups. ^d “Twist angle” of the dimethyl-amino group, defined as the average of the dihedral angles C_{Me}NC₄C₃ and C_{Me}NC₄C₃. ^e From a model potential fitted to describe the low-lying vibrational progressions in the gas-phase spectrum (ref 53). ^f “Out-of-plane angle” of the dimethyl-amino group, defined as the angle of the C₄N bond with respect to a plane given by C₄, C₃, and C₃. ^g Derived from macroscopic quantities (dielectric constant, refractive index) in dioxane at 25 °C (ref 10). ^h From time-resolved microwave conductivity measurements in 1,4-dioxane (ref 10). ⁱ Vertical energy separation from the ground state. ^j Maximum of dispersed emission of jet-cooled DMABN (ref 54). ^k Maxima of ICT fluorescence bands in 1,4-dioxane/benzene/cyclohexane (ref 10). ^l Adiabatic excitation energy (rel to the ground-state minimum). ^m Position of the 0–0 transition. ⁿ Laser-induced fluorescence (LIF) excitation spectrum in the gas phase (ref 55).

All RI-CC2 calculations have been carried out using the TZVPP basis set^{46,47} and the corresponding auxiliary basis sets for the RI approximation.⁴⁷ All valence electrons were included in the correlation treatment, only the 1s² cores of the carbon and nitrogen atoms were kept frozen. At the resulting equilibrium structures, vibrational spectra were calculated numerically from the analytic gradients using central differences in Cartesian coordinates with displacements of ±0.01a₀. Isotope shifts of certain bands were identified from the overlap of the corresponding normal mode vectors, and assignments of normal modes to certain group vibrations were based on the vibrational potential energy distribution. We note that (as in comparable studies) the vibrational frequencies were derived from the harmonic force field and thus include neither anharmonicity corrections nor solvent effects. When these frequencies are used to assign experimental spectra in the later sections, these additional error sources have to be kept in mind. For differential properties such as isotope shifts, some error cancellation and thus better comparability can be expected.

To test for possible multireference effects, CASSCF calculations were carried out employing small SVP⁴⁸ basis sets. Above that, the convergence of the coupled-cluster hierarchy was studied for selected cases employing CC2, CCSD, CCSDR(3) (noniterative perturbative correction for the effect of connected triples in excited states⁴⁹), and the SVP basis. CASSCF and the latter coupled-cluster calculations were carried out with the DALTON program package.⁵⁰

We also investigated the impact of additional diffuse functions in the basis set. Nearly no changes in energy, structure, and dipole moments were found for the structures discussed in this paper. We

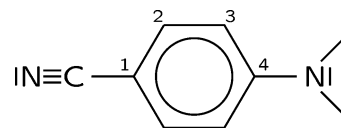


Figure 1. Numbering of the ring atoms as used in the text. Symmetry-equivalent atoms are referred to with a prime, e.g., C₂ and C₂'. In the entire text, the molecule is assumed to be oriented with its long axis along the z-axis and phenyl-ring in the xz plane.

note that only in the Franck–Condon region (i.e., in the calculation of vertical excitation energies) a notable effect of diffuse basis functions was found.

3. Results

Calculated structures, dipole moments, and energy separations for the ground electronic state and the two lowest lying singlet-excited electronic states of DMABN are summarized in Table 1, together with available experimental data. Detailed discussions of the results are given in the subsequent sections. Figure 1 displays the atom numbering used in the following.

3.1. Ground State. A. Structure. Both X-ray diffraction in the crystalline phase⁵¹ and microwave spectroscopy in the gas phase⁵² have established a slight pyramidalization of the amino group of DMABN. Wagging (or amino-inversion) angles ω of

- (44) Vahtras, O.; Almlöf, J. E.; Feyereisen, M. W. *Chem. Phys. Lett.* **1993**, *213*, 514.
 (45) Hättig, C.; Köhn, A. *J. Chem. Phys.* **2002**, *117*, 6939–6951.
 (46) Schäfer, A.; Huber, C.; Ahlrichs, R. *J. Chem. Phys.* **1994**, *100* (8), 5829–5835.
 (47) Weigend, F.; Häser, M.; Patzelt, H.; Ahlrichs, R. *Chem. Phys. Lett.* **1998**, *294*, 143–152.
 (48) Schäfer, A.; Horn, H.; Ahlrichs, R. *J. Chem. Phys.* **1992**, *97* (4), 2571–2577.
 (49) Christiansen, O.; Koch, H.; Jørgensen, P. *J. Chem. Phys.* **1996**, *105*, 1451–1459.

- (50) Helgaker, T.; Jensen, H. J. A.; Jørgensen, P.; Olsen, J.; Ruud, K.; Ågren, H.; Auer, A. A.; Bak, K. L.; Bakken, V.; Christiansen, O.; Coriani, S.; Dahle, P.; Dalskov, E. K.; Enevoldsen, T.; Fernandez, B.; Hättig, C.; Hald, K.; Halkier, A.; Heiberg, H.; Hettner, H.; Jonsson, D.; Kirpekar, S.; Kobayashi, R.; Koch, H.; Mikkelsen, K. V.; Norman, P.; Packer, M. J.; Pedersen, T. B.; Ruden, T. A.; Sanchez, A.; Saue, T.; Sauer, S. P. A.; Schimmelpfennig, B.; Sylvester-Hvid, K. O.; Taylor, P. R.; Vahtras, O. *Dalton—an electronic structure program*, release 1.2; 2001.
 (51) Heine, A.; Herbst-Irmer, R.; Stalke, D.; Kühnle, W.; Zachariasse, K. A. *Acta Crystallogr.* **1994**, *B50*, 363–373.
 (52) Kajimoto, O.; Yokoyama, H.; Ooshima, Y.; Endo, Y. *Chem. Phys. Lett.* **1991**, *179*, 455–459.

Table 2. Calculated (CC2/TZVPP) Harmonic Frequencies and Isotopic Shifts for Selected Modes of the Ground State of DMABN in Comparison to Experimental Observations (for the Definition of the Isotopomers, See Text)

mode	DMABN			DMABN- ¹⁵ N		DMABN- <i>d</i> ₆		DMABN- <i>d</i> ₂		assignment ^g	
	ν_{ca}^a	I_{ca}^b	ν_{ob}^c	I_{ob}^d	$\Delta\nu_{ca}^e$	$\Delta\nu_{ob}^f$	$\Delta\nu_{ca}^e$	$\Delta\nu_{ob}^f$	$\Delta\nu_{ca}^e$		$\Delta\nu_{ob}^f$
12 a'	798	(2)	788, ^h 785 ⁱ		0	0 ^h	-12	-11 ^h	-16		1, 6a
15 a'	963	(8)	944, ^j 944 ^h , 943 ⁱ	w	-6	-6 ^j , -7 ^h	-120	-111 ^h	+5	+10 ⁱ	ν_{N-Me}^s
16 a'	1014	(0)	1005 ⁱ , 1003 ⁱ	vw	0	0 ^j , -1 ⁱ	0	0 ⁱ	-158	-111 ⁱ	12, 19a
17 a'	1152	(27)	1171 ^j , 1166 ⁱ	m	-4	0 ^j , 0 ^h	-237	-133 ⁱ	+1	+3 ^j	ρ_{Me}
18 a'	1194	(9)	1180 ^j , 1179 ^h , 1180 ⁱ	sh	0	0 ^j , -1 ^h	-149	+1 ^j , -1 ^h (? ^k)	-1		ρ_{Me} , 1
19 a'	1201	(6)			0		-1	+1 ^j , -1 ^h (? ^k)	+3		δ_{C-H}
20 a'	1236	(0)	1227 ^h , 1227 ⁱ		0	0 ^h	1	0 ^h	-160		δ_{C-H} , ν_{Ph-CN} , 8a, 12
14 a''	1277	(13)	1229 ^j	m	-17	-13 ^j	-19	-20 ^j	-61	-75 ^j	ν_{N-Me}^s
16 a''	1401	(0)	1324 ^h , 1323 ⁱ		-5	-6 ^h	-5	-2 ^h	-16		14, 19b
21 a'	1390	(63)	1372 ^j , 1377 ^h , 1370 ⁱ	s	-16	-13 ^j , -13 ^h	0	+8 ^j , 0 ^h	-12	-8 ^j	ν_{Ph-N} , ν_{N-Me}^s , δ_{C-H}
22 a'	1483	(10)	1449 ^j , 1446 ⁱ		0	-1 ^j , 0 ⁱ	-322	-314 ⁱ	-17	-18 ^j	δ_{Me}
25 a'	1555	(76)	1529 ^j , 1527 ^h , 1522 ⁱ	s	-5	-5 ^j , -5 ^h	-11	-7 ^j , -7 ^h	-8	-17 ^j	δ_{C-H} , 19a, ν_{Ph-N}
21 a''	1579	(1)	1546 ^h , 1545 ⁱ		-1	-1 ^h	-1	0 ^h	-13		8b
26 a'	1645	(100)	1609 ^j , 1606 ^h , 1600 ⁱ	vs	-1	0 ^j , 0 ^h	-2	-3 ^j , -3 ^h	-12	-11 ^j	8a
27 a'	2104	(12)	2219 ^h , 2217 ^j , 2213 ^m		0	0 ^h	0	0 ^h	0		ν_{CN}

^a Calculated harmonic frequency in cm^{-1} . ^b Calculated IR intensity in percent of most intense band. ^c Observed fundamental band in cm^{-1} . ^d Qualitative IR intensity from refs 30 and 56. ^e Calculated frequency shift in cm^{-1} . ^f Observed frequency shift in cm^{-1} . ^g Numbers refer to the Wilson modes (ref 57) of the C_6 scaffold, and δ_{C-H} always denotes in-plane bending of the phenyl-hydrogens. ^h Resonant Raman in methanol from ref 29. ⁱ Nonresonant Raman in solid phase from ref 29. ^j IR in acetonitrile from refs 30 and 31. ^k 18a' and 19a' may both contribute to the band of natural DMABN, whereas 18a' gives rise to the band seen for DMABN-*d*₆. ^l IR in acetonitrile from ref 59. ^m IR in methanol from ref 59.

11.9° and around 15°, respectively, have been reported^{51,52} (see footnote of Table 1 for the definition of this internal coordinate). Theoretical studies have come to similar results, but it turned out that basis sets of triple- ζ quality were necessary to obtain satisfactory results for the pyramidalization angle.¹⁸

The CC2/TZVPP calculations yield a wagging angle of 23°. The inversion barrier between the two equivalent minima amounts to only 0.009 eV (71 cm^{-1}), which is about double the (harmonic) zero-point energy of the associated normal mode of the distorted molecule. At finite temperatures, this barrier can thus be easily overcome. Above that, the calculated dipole moment of the C_{2v} structure is slightly increased to 7.7 D (as compared to 7.4 D for the C_s structure), which might decrease the barrier height in solution phase due to solvation effects, possibly leading to a planar minimum structure. These dipole moments are in reasonable agreement with an experimental estimate derived from measurements on solutions of DMABN in dioxane.¹⁰ The phenyl moiety shows a quinoidal distortion along the long molecular axis (i.e., short C_2-C_3 and $C_2'-C_3'$ bonds). In addition, the bond towards the dimethyl-amino group is shorter than expected for a pure C-N single bond, indicating a stabilizing interaction between the nitrogen lone pair and the π -system.

As compared to the structure parameters derived from X-ray diffraction⁵¹ the calculated bond lengths are typically 1 pm larger which is within the experimental error bars. The theoretical prediction for the cyano group bond, however, is clearly too large by 3.7 pm. This is a shortcoming of CC2 which is known to give too weak triple bonds.^{38,39} But it was shown in ref 39 for the example of HCN that differential properties such as adiabatic excitation energies and changes in the bond length or in the harmonic vibrational frequency are still reproduced very well.

B. Vibrational Spectrum. Experimentally, vibrational frequencies of DMABN have been studied by both Raman²⁹ and infrared⁵⁶ (IR) techniques in solution phase. Apart from natural DMABN, further isotopomers were measured in these studies, of which three are considered in this work: DMABN-¹⁵N in which the nitrogen of the dimethyl-amino group has been

replaced by its heavier isotope, DMABN-*d*₆ in which the six hydrogen atoms of the methyl groups are replaced by deuterium, and DMABN-*d*₂ in which two hydrogen atoms attached to C_3 and C_3' are substituted by deuterium.

Table 2 summarizes the calculated results from the present work together with experimental data. The calculated frequencies can very consistently be assigned to the observed bands (within the limitations indicated in section 2). The assignments are supported by the calculated isotopic shifts and the IR intensities which both are in very good agreement with experimental observations. The interpretation in terms of more or less localized group vibrations is hampered by the often strongly mixed character of the normal modes. The assignments in the last column of Table 2 should thus not be taken too literally as they often indicate only the most important of the contributing coordinates. It has therefore been criticized in the literature³¹ that, barely on the observations of certain shifts of vibrational frequencies upon excitation, no necessary conclusions can be drawn on the decrease or increase of certain bond strengths. We will show, however, that the critical modes discussed, e.g., in ref 29 show shifts which, fortuitously or not, indeed reflect the change in the underlying force constants.

We will in particular discuss the bending and stretching modes of the C_6 scaffold (designated according to Wilson's notation^{57,58}) that reflect the electronic structure of the π -system, as well as the stretching mode of the bond connecting the cyano group and the phenyl ring (called Ph-CN bond hereafter), the stretching mode of the bond between the phenyl ring and the

(53) Saigusa, H.; Miyakoshi, N.; Mukai, C.; Fukagawa, T.; Kohtani, S.; Nakagaki, R.; Gordon, R. *J. Chem. Phys.* **2003**, *119*, 5414–5422.

(54) Lommantzsich, U.; Gerlach, A.; Lahmann, C.; Brutschy, B. *J. Phys. Chem. A* **1998**, *102*, 6421–6435.

(55) Pérez Salgado, F.; Herbich, J.; Kunst, A. G. M.; Rettschnick, R. P. H. *J. Phys. Chem. A* **1999**, *103*, 3184–3192.

(56) Okamoto, H. *J. Phys. Chem. A* **2000**, *104*, 4182–4187.

(57) Wilson, Jr., E. B. *Phys. Rev.* **1934**, *45*, 706–714.

(58) These are the six stretching (1, 8a/b, 14, and 19a/b) and three in-plane bending (6a/b, and 12) modes of the C_6 -scaffold. We note that 19a/b tends to mix strongly with 18a/b (hydrogen in-plane bending). Actually, in natural benzene, 19a/b is predominantly a hydrogen in-plane bending mode, whereas, for C_6D_6 , it is dominated by the stretching mode. In the present work, 19a/b is understood to be the stretching mode.

Table 3. Calculated Force Constants (in N m^{-1}) for Selected Bonds in DMABN (for Numbering of the Atoms, See Figure 1)

bond	ground state	LE state	ICT state ^a
C ₃ –C ₄	363	321	277 (286)
C ₂ –C ₃	384	292	410 (411)
C ₁ –C ₂	342	312	305 (282)
C≡N	785	774	740 (727)
Ph–CN	313	301	331 (338)
Ph–N	374	321	221 (262)
N–C _{Me}	286	269	259 (240)

^a Values for C_{2v} structure are given in parentheses.

dimethyl-amino group (Ph–N bond), and the cyano group stretching mode. The latter three are expected to be most sensitive to changes in the electronic system due to the ICT process, and special focus was put on them in several experimental studies.^{29–33}

The ring modes of ground state DMABN appear at the frequencies expected for benzene derivatives. The ring breathing mode and the 19a mode show up at somewhat low frequencies as they strongly mix with bending modes, 6a and 12. The band at 1555 cm^{-1} , experimentally observed around 1525 cm^{-1} , has in the literature partly been interpreted³⁰ as the 19a carbon–carbon stretching mode. At variance, our analysis indicates a predominant in-plane bend of the phenyl hydrogens with considerable admixture of 19a, consistent with the ordering of these modes in natural benzene (see also ref 58).

A more clear-cut picture arises from the force constants for the three symmetry-unique C–C bonds that can be found in Table 3. Their size is comparable with the C–C force constant found in benzene (361 Nm^{-1} with CC2/TZ2P,⁶⁰ best experimental estimate⁶¹ 350 Nm^{-1}). The slightly quinoid character of the ground state π -system is apparent from the force constants, as the C₂–C₃ bond is the strongest of these.

At 1236 cm^{-1} (expt 1227 cm^{-1}) a band appears that can be assigned to the Ph–CN stretching mode, whereas the Ph–N stretching mode is found at 1390 cm^{-1} (expt 1370 cm^{-1}). Both vibrations, in particular the first one, couple strongly with in-plane modes of the phenyl hydrogen atoms, as can be seen from isotopic shifts observed for DMABN-*d*₂ (see Table 2). The force constant of 374 Nm^{-1} in Table 3 suggests a partial double bond character of the Ph–N bond, if the value of 286 Nm^{-1} for the N–C_{Me} group bond is taken as reference for a typical C–N single bond.

The cyano group stretching mode is located at 2104 cm^{-1} (expt 2219 cm^{-1}). This somewhat too low lying theoretical prediction goes along with the too long triple bond calculated for that group (see structure section above) and is not unexpected for CC2.^{38,39} The cyano vibration is well separated from other modes, however, such that this underestimation has nearly no effect on the other vibrational modes for which the CC2 model is expected to perform much better.

3.2. General Features of the Excited State Hypersurfaces.

We started with an investigation of the minimum energy path of the lowest excited states of DMABN along the twist coordinate τ , which in nearly all preceding theoretical studies

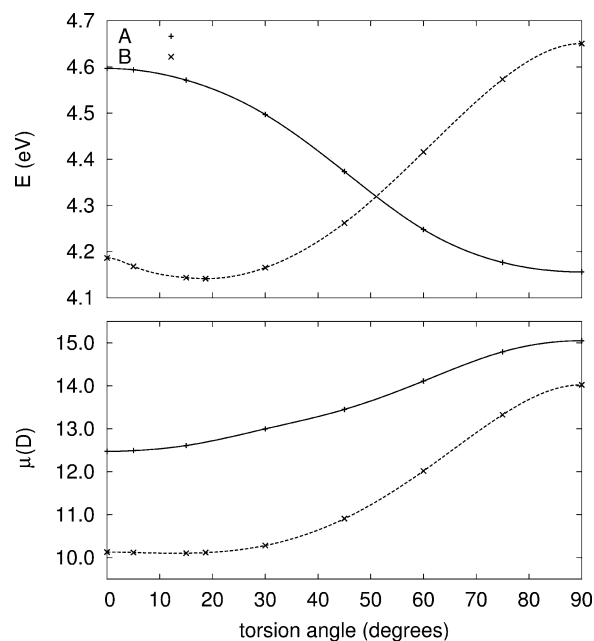


Figure 2. Calculated potential energy (eV) and dipole moment (Debye) of the two lowest singlet-excited states of DMABN as a function of the torsion angle τ along the C₂ symmetric path. The energy is quoted relative to ground state minimum.

was considered the most important degree of freedom (see, e.g., refs 12, 14–17, 19–23, 25, 26). Geometry optimizations were carried out, where, except for a fixed twisting angle and imposing C₂ symmetry,⁶² the structure of the excited states was completely relaxed. The two lowest states now transform according to the A and the B representation of the C₂ point group. The resulting potential energy curves and the dependence of the dipole moments on τ are given in Figure 2.

We find the B state to possess a shallow double minimum at $\pm 19^\circ$ with a small barrier of less than 0.05 eV. At small angles, the dipole moment does nearly not depend on the torsion coordinate. It is, however, pronouncedly higher than in the ground state (10 D vs 7 D) and increases significantly as τ approaches 90° . The A state, on the other hand, shows a pronounced lowering of its energy for τ approaching 90° , accompanied by a marked increase in its dipole moment. The A and B states cross at around 50° , where it should be noted that both curves are minimum paths such that the crossing point in Figure 2 does not directly correspond to the actual intersection. This state intersection has been observed in a number of previous theoretical studies,^{12,14–17,19,20,22,23,25,26} although, among the studies including dynamic correlation effects, the present work and the TDDFT study of Rappoport and Furche²⁶ were the first to obtain both energy and minimum geometry at the same level of theory, thus reducing the arbitrariness in the choice of methods to a minimum.

Certainly, as most experiments on dual fluorescence are carried out in solution, the question arises how solvent effects alter the potentials shown in Figure 2. From the group of Tomasi,^{22,23} results from the polarizable continuum model (PCM) are reported, while Sudholt et al.¹⁷ employed molecular dynamics simulations. In both cases, the ICT state (the A state in Figure 2) is predicted to shift down all along the twist path,

(59) Kwok, W. M.; George, M. W.; Grills, D. C.; Ma, C.; Matousek, P.; Parker, A. W.; Phillips, D.; Toner, W. T.; Towrie, M. *Angew. Chem., Int. Ed.* **2003**, *42*, 1826–1830.

(60) Christiansen, O.; Stanton, J. F.; Gauss, J. *J. Chem. Phys.* **1997**, *108*, 3987–4001.

(61) Goodman, L.; Ozkabak, A. G.; Thakur, S. N. *J. Phys. Chem.* **1991**, *95*, 9044–9058.

(62) This was done for simplicity. In sections 3.3 and 3.4, we will investigate whether further symmetry lowering occurs.

as it is expected from its higher dipole moment.⁶³ So far, however, not much experience exists with the accuracy of such solvation models, and certainly further work in this direction is desirable.

As a first conclusion, our results summarized in Figure 2 support the TICT hypothesis in the sense that only along this coordinate a significant change in the energetics of the two lowest singlet excited states can be observed. At 0°, where a PICT-like state would be expected, no indication for a (at least local) minimum is found. Though the phenyl moiety is quinoid at all twist angles, we do not observe a significant shortening of the C₄–N bond which eventually leads to the structure proposed by the PICT model. On the contrary, the bond length increases from 142.0 pm ($\tau = 90^\circ$) to 143.1 pm ($\tau = 0^\circ$) and is significantly larger than in the ground state (137.7 pm). We will give further comments on that issue in section 4. Before, however, we will discuss the structures of the two excited-state minima in some detail.

3.3. Locally Excited State. A. Structure. The minimum structure (see Table 1) has C₂ symmetry, as confirmed by force-constant calculations discussed in the subsequent paragraph. The carbon–carbon bonds of the phenyl moiety are pronouncedly longer than those in the ground state, and the C₆ ring is distorted in an anti-quinoid fashion (i.e., it exhibits long C₂–C₃ bonds). The bond toward the dimethyl-amino group is only slightly longer than that in the ground state, and the group itself (showing a planar conformation at the nitrogen atom) is twisted by 19° along the torsion coordinate τ . Our findings cast considerable doubt on the accuracy of TDDFT for this state which predicts a nearly flat line for the minimum energy path, with a local minimum at 32.5° and a global minimum at 90°.²⁶ The shallow potential, suggesting a nearly free rotation of the dimethyl-amino group is also in conflict with recent gas-phase spectra of this state⁵³ which are discussed below. As our results for the dipole moment suggest (see Figure 2), the LE gains increasing ICT character for larger torsion angles τ which explains the obvious failure of TDDFT.

From experimental studies only few estimates exist concerning the structure. They mainly focus on the torsion angle for which values between 0° and 30° have been put forward,^{52,53,55,64} whereas in most studies the amino inversion angle is assumed to be 0° (as suggested in ref 52). In a recent study, the vibrational progressions of the LE → S₀ transition were carefully investigated and fitted to a model double minimum potential of the form⁵³

$$V(\tau) - V_0 = V_2/2(1 - \cos 2\tau) + V_4/2(1 - \cos 4\tau)$$

for the torsional motion, resulting in a minimum at $\tau_0 = \pm 26^\circ$. We note that the shape of the LE potential in Figure 2 (state B) turns out to be too complicated to be fitted properly with the above model potential. To reproduce both the barrier height (at $\tau = 0$) and the correct position of the minimum, very high oscillating terms are needed (while, e.g., the ICT state potential

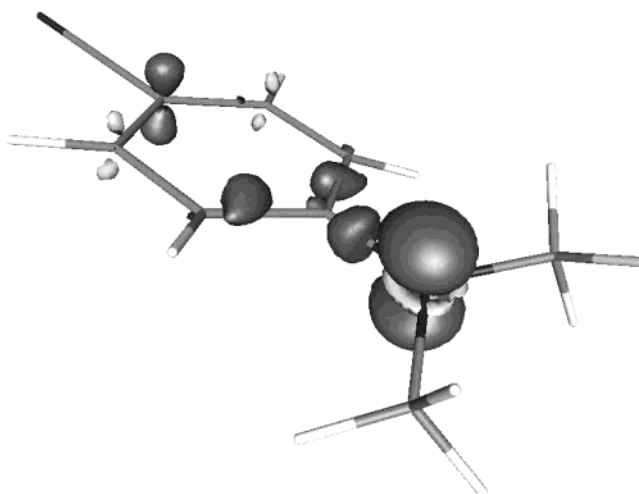


Figure 3. Difference density (LE state density minus ground state density) at the LE state minimum structure. A dark shaded isosurface surrounds areas of decreasing electron density; a light shaded isosurface is plotted at areas of increasing electron density. All difference density plots use the same isovalue of $\pm 0.02a_0^{-3}$.

from Figure 2 is already very well fitted by a single cosine function). The two-parameter potential for the LE state therefore tends to give too large values for τ_0 if a proper barrier height is to be reproduced, on which the vibrational levels are presumably more sensitive.

In accordance with experimental data, the LE state possesses a dipole moment of about 10 D which is somewhat larger than in the ground state. The difference-density map in Figure 3 illustrates the partial charge-transfer character of the LE state. It shows that a significant amount of electron density is removed from the nitrogen lone pair thus explaining the planarity of that group. The excess electron density is partly delocalized in the π -system of the phenyl group (mainly on atoms C₂ and C_{2'}), and also the electron density in the dimethyl-amino σ -system is increased. The cyano group, on the other hand, is not significantly involved in this transition.

The estimated 0–0 transition (using the harmonic CC2 force fields for ground and excited state) amounts to 3.96 eV which is, considering the usual accuracy of the employed method,³⁹ somewhat unexpectedly close to the experimental number of 3.998 eV^{53,55} (see also section 3.5). The calculated vertical emission energy is 3.78 eV. This compares well with the dispersed emission maximum of jet-cooled DMABN⁵⁴ which amounts to 3.76 eV. We note that, despite the mentioned problems with the torsion barrier, the TDDFT calculations also result in a value of 3.76 eV for the LE emission.²⁶

B. Vibrational Spectrum. The vibrations of the ring scaffold reflect the anti-quinoid character of the state. In particular, the Kekulé mode 14 becomes the energetically highest-lying ring-stretching mode in our calculations, lying now at 1536 cm⁻¹, whereas 8a and 8b shift down considerably. This interpretation is supported by the force-constants in Table 3. We find on the average weaker bonds than in the ground state, and the quinoid C₂–C₃ bond is clearly the weakest of the three.

In the experimental spectra, the identification of the ring modes is difficult, since the LE state has a short lifetime in solution and experimental spectra still have a rather low resolution. The experimental Raman spectra^{32,33} feature four bands at around 980 cm⁻¹, 1050–1200 cm⁻¹, 1300–1500 cm⁻¹,

(63) Gorse and Pesquer (ref 11) also tried to model solvation effects based on semiempirical AM1 calculations. Their in vacuo results, however, yielding potential energy curves that for both LE and ICT increase strongly as the dimethyl-amino group is twisted, are in conflict with more elaborate ab initio results such as the present work and put serious doubts on the applicability of the AM1 method.

(64) Grassian, V. H.; Warren, J. A.; Bernstein, E. R. *J. Chem. Phys.* **1988**, *90*, 3994–3999.

Table 4. Calculated (CC2/TZVPP) Harmonic Frequencies and Isotopic Shifts for Selected Modes of the LE State of DMABN in Comparison to Experimental Observations (for the Definition of the Isotopomers, See Text)

mode	DMABN		DMABN- ¹⁵ N		DMABN- <i>d</i> ₆		DMABN- <i>d</i> ₂		assignment
	ν_{ca}^a	ν_{ob}^b	$\Delta\nu_{ca}^c$	$\Delta\nu_{ob}^d$	$\Delta\nu_{ca}^c$	$\Delta\nu_{ob}^d$	$\Delta\nu_{ca}^c$	$\Delta\nu_{ob}^d$	
9 a	788		0		-14		-22		1, 6a
10 a	940		-5		-104		+8		ν_{N-Me}^s , 1
11 a	996	973 ^e	0		-1		-158		12, 19a
15 b	1014		0		-1		-151		19b, δ_{C-H}
14 a	1156	1113 ^f , 1117 ^e	0		-3	-11 ^f	-319		δ_{C-H} , 8a
15 a	1181	1168 ^f , 1174 ^e	0		-3	-2 ^f	-8		ν_{Ph-CN} , 12, δ_{C-H}
18 b	1184		-5		-6		+3		8b
20 b	1325	1325 ^f (? ^g)	-3		3	-40 ^f (? ^g)	-186		δ_{C-H}
16 a	1353	1357 ^f , 1334 ^e	-18		-20	-6 ^f	-7		ν_{Ph-N} , ρ_{Me}
21 b	1377	1399 ^{*h}	-3	-1 ^h	-2		-11	-1 ^h	δ_{C-H}
17 a	1421	1416 ^f , 1423 ^e , 1415 ^h	0	0 ^h	-316		+13	+1 ^h	δ_{Me}
18 a	1455	1467 ^f , 1460 ^e (? ⁱ)	0		-5	-13 ^f (? ⁱ)	-22		δ_{C-H}
23 b	1482	1481 ^{*h}	0	0 ^h	-415		0	- ^j	δ_{Me}
19 a	1485	1467 ^f , 1460 ^e (? ⁱ)	0		2	-13 ^f (? ⁱ)	-2		8a, δ_{C-H}
25 b	1536		0		-5		-3		14
22 a	2073	2176 ^f , 2181 ^e	0		0	+2 ^f	0		ν_{CN}

^a Calculated harmonic frequency in cm^{-1} . ^b Observed fundamental band in cm^{-1} . ^c Calculated frequency shift in cm^{-1} . ^d Observed frequency shift in cm^{-1} . ^e Time-resolved resonance Raman in cyclohexane with 615 nm probe (from ref 32). ^f Time-resolved resonance Raman in cyclohexane with 600 nm probe (from ref 33). ^g Very weak feature. ^h Time-resolved infrared spectroscopy in cyclohexane (from ref 31). A star indicates experimental evidence for a nontotally symmetric character of the vibrational mode. ⁱ Rather broad feature, may include contributions from several bands up to 25b. ^j Band vanishes on substitution (ref 31).

and 2180 cm^{-1} . The two broad bands are not very well resolved into single contributions, and the subbands identified by the authors of refs 32 and 33 (as used in Table 4) carry relatively large uncertainties.

The band maximum at 973 cm^{-1} may be tentatively assigned to the mixed 12/19a mode. No isotope information is available for this band, thus the assignment is based on the theoretical prediction that both the 12/19a mode and the nearby lying symmetric stretching mode of the two nitrogen-methyl bonds are shifted to lower frequency after electronic excitation (by -18 cm^{-1} and -23 cm^{-1} , respectively); these modes are observed at 1005 cm^{-1} and 944 cm^{-1} in the ground state experiment; therefore only the above assignment seems consistent with the calculations. The ring modes 8a and 14 may contribute to the broad band group at $1300\text{--}1500\text{ cm}^{-1}$, but no certain assignment can be made.

The Ph-CN stretching mode is calculated at 1181 cm^{-1} , and as in the ground state, it includes coupling with in-plane vibrations of the phenyl hydrogen atoms. Relative to the ground state, it is shifted down by -55 cm^{-1} . The band found at 1168 and 1174 cm^{-1} in time-resolved resonance Raman experiments^{32,33} may be assigned to this normal mode. With some caution, because of the different solvents in the ground and in the excited state measurements,⁶⁵ we may derive a red-shift of about -53 to -59 cm^{-1} relative to the ground state, in close agreement to the calculated value.

The Ph-N stretching mode is expected in the lower part of the band group at $1300\text{--}1500\text{ cm}^{-1}$. In their first publication,³² Kwok et al. quoted a band maximum at 1334 cm^{-1} , while, in the more recent work,³³ two bands, a weak one at 1325 cm^{-1} and stronger one at 1357 cm^{-1} , were reported. The band system undergoes significant changes upon $-d_6$ substitution,³³ but it is actually difficult to obtain reliable estimates of isotopic shifts due to the rather low resolution of the experimental spectra. According to our calculations, there are two bands in this region, an antisymmetric in-plane hydrogen bending mode at 1325 cm^{-1}

and the Ph-N stretching mode at 1353 cm^{-1} . The calculated isotopic shifts are not compatible with the experimental ones (see Table 4) which, however, contain large uncertainties (in particular the lower one of the bands is only a "weak feature of uncertain assignment"³³) and therefore neither validate nor invalidate our assignment. The relative shift of the Ph-N mode, as compared to the ground state, is calculated as -37 cm^{-1} , while, from the above experimental band maxima of either 1334 cm^{-1} or 1357 cm^{-1} , we can estimate a shift between -24 and -47 cm^{-1} . This supports the hypothesis that at least parts of the observed broad band are due to this normal mode.

The red-shifts of both bands, attributed to the Ph-CN and the Ph-N bond stretching, indicate a weakening of these bonds, and also the force constants in Table 3 support this interpretation. Note, however, that no simple relation between the lowering of the force constants and the frequency shifts can be found, indicating that changes in the coupling with other modes have, too, a strong influence on the observed shifts.

The experimentally observed band around 2180 cm^{-1} can be unequivocally attributed to the cyano stretching mode, which at the CC2 level is again underestimated (2073 cm^{-1}). The shift of -31 cm^{-1} upon excitation, however, is in good agreement with the experimental number lying between -43 cm^{-1} and -38 cm^{-1} (with some caution due to different solvents as mentioned above).

From the experimental gas-phase spectra, further modes in the low-frequency region can be identified. However, as overtones and combination bands are present (cf. the assignments given in ref 53), an interpretation would require a careful simulation of the vibronic spectrum, which is beyond the scope of the present work. We only note that Saigusa et al.⁵³ assigned the progression at 75.5 cm^{-1} to a torsional mode. The band is reported to shift down by -9.6 cm^{-1} upon d_6 substitution. This compares well with our computed result, a harmonic frequency of 86 cm^{-1} for this mode and a red-shift of -9 cm^{-1} upon d_6 substitution.

3.4. Intramolecular Charge-Transfer State. A. Structure.

In contrast to the LE minimum on the C_2 path, the ICT

(65) It may be added that for the Raman experiments the calibration error in the absolute frequencies is $\pm 5\text{ cm}^{-1}$ (refs 29, 32) to $\pm 10\text{ cm}^{-1}$ (ref 33).

minimum, actually possessing C_{2v} symmetry at 90° , turns out to be a saddle point in our calculations. The symmetry-breaking coordinate is a pyramidalization of the carbon atom adjacent to the dimethyl-amino group (atom C_4 , see Figure 1). Additionally, we find that the methyl group which is syn to the phenyl moiety rotates such that one hydrogen points toward the middle of the ring. The latter, however, is only a minor detail as the energetic effect of the rotation is very small.

In the low-symmetry structure, the bond between the ring and the dimethyl-amino group is elongated by 2 pm as compared to the C_{2v} structure. In both structures, the phenyl moiety has a marked quinoidal character with two very short double bonds between the carbon atoms C_2 and C_3 (and C_2' and C_3' , respectively), whereas the C_1 – C_2 and C_3 – C_4 bonds have lengths close to single bonds (see Table 1). Including zero-point vibrational effects, the stabilization energy of the C_s structure, however, is barely 0.05 eV which may in solution phase be overcome by stabilization effects due to the pronouncedly higher dipole moment of the C_{2v} structure (see Table 1).

In contrast to that, the energetic effect of the distortion on the ground-state energy is considerable, and whereas we calculate a vertical emission energy of 3.3 eV for the C_{2v} -symmetric structure, barely 2.5 eV are found for the low-symmetry structure. The latter value does not compare well with experimental estimates, which suggest values above 3 eV for nonpolar solvents. On the other hand, we have to keep in mind that we calculated a very shallow double minimum potential for the ICT state associated with a harmonic vibrational frequency of 52 cm^{-1} at each of the minima. These modes are readily populated at finite temperatures, and emission may also take place from vibronically excited states,⁶⁶ suggesting that the form function of the emission may be more complex and that its maximum cannot be easily derived from vertical energy separations.

The carbanion-like distortion is found for all values of τ for the C_2 -symmetric A state in Figure 2, thus stabilizing the state on the average by 0.05 to 0.1 eV. It is interesting to note that there is an interesting implication for $\tau = 0$: As can be seen from Figure 4, the distortion leads to another possible intersection of A and B at an out-of-plane angle around 30° (note that as in Figure 2 also in Figure 4 no vertical energy separations are shown). Thus this motion constitutes another possible decay path after initial vertical excitation into the A state which may be of importance for quantitative simulations of the observations in recent femtosecond experiments.^{67,68}

As for the minimum structure at $\tau = 90^\circ$, the dipole moment of the ICT state decreases along the out-of-plane coordinate and some care is appropriate with respect to the structure of this state in solution phase. We conjecture that solvent interactions may stabilize the C_2 high-symmetry path but that still a large amplitude motion along the out-of-plane mode will be possible.

In Figure 5, the difference density of the ICT state relative to the ground state is depicted. It illustrates the apparently much stronger charge-transfer character of this transition, as compared

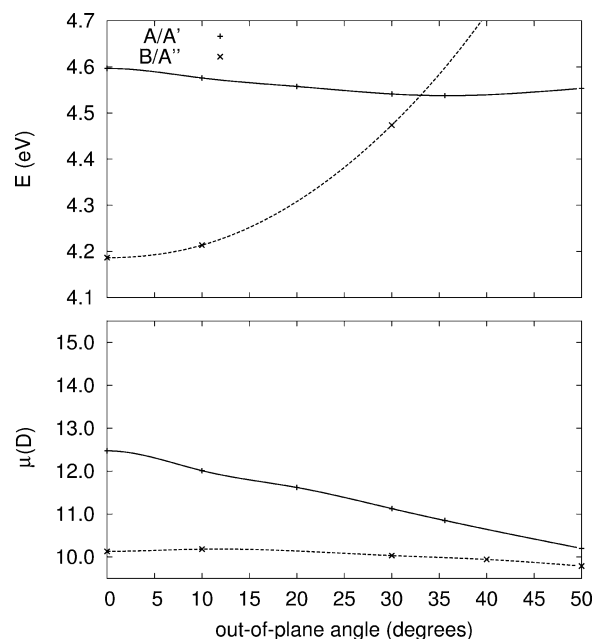


Figure 4. Calculated potential energy (eV) and dipole moment (Debye) of the two lowest singlet-excited states of DMABN as a function of the out-of-plane angle ϕ at $\tau = 0$ (C_s symmetric path). The energy is quoted relative to the ground state minimum.

to the LE state, Figure 3. Figure 5a shows that the electron density is shifted from the nitrogen lone pair to the phenyl group, where it is mainly localized on C_4 , C_1 and the nitrogen atom of the cyano group play only a minor role as acceptors; i.e., the system tries to minimize the charge separation. Finally, Figure 5b illustrates the driving force of the out-of-plane distortion, a carbanion-like localization of the excess charge in a lone pair of C_4 . We have found this effect in comparable ICT states of related molecules too, as in aniline and 4-amino-benzonitrile (ABN). The stabilization energy due to the distortion decreases in the sequence aniline, ABN, DMABN underlining the importance of both electronic (through the cyano group) and steric (through the methyl groups) effects. It may be argued that CC2 is not be capable of correctly describing the electronic effect of the cyano group as it predicts an obviously too long bond. We will therefore in section 3.5 substantiate the predictions of CC2 with results from more elaborate methods.

In contrast to our result, Rappoport and Furche obtain a C_{2v} symmetric TICT state in their TDDFT study.²⁶ This is not unexpected and can be understood as a direct consequence of the employed density functional's tendency to give too low energies for charge-transfer states, as already mentioned in the Introduction. It can be seen from the dipole moments in Table 1 that the C_{2v} symmetric structure has indeed a stronger charge-transfer character than that of the C_s symmetric one.

B. Vibrational Spectrum. As discussed above, we expect that in solution phase the ICT state has a more or less C_{2v} symmetric structure. As intense ICT emission is only observable in solution, experimental data for vibrational modes is available for these experimental conditions only. A comparison with vibrational frequencies derived theoretically for the C_{2v} structure seems thus to be more adequate. In Table 5, results for both structures are listed, but we will for simplicity only quote the vibrational frequencies from the C_{2v} structure in the subsequent discussion. Only for the modes $7 a_1$, $9 b_2$ and $11 b_2$ somewhat larger differences between the frequencies calculated for the

(66) That vibronically excited states are involved in the ICT emission process has already been discussed in connection with the temperature dependence of the ICT band; see ref 4 and references therein.

(67) Fuß, W.; Pushpa, K. K.; Rettig, W.; Schmid, W. E.; Trushin, S. A. *Photochem. Photobiol. Sci.* **2002**, *1*, 255–262.

(68) Trushin, S. A.; Yatsuhashi, T.; Fuß, W.; Schmid, W. E. *Chem. Phys. Lett.* **2003**, *376*, 282–291.

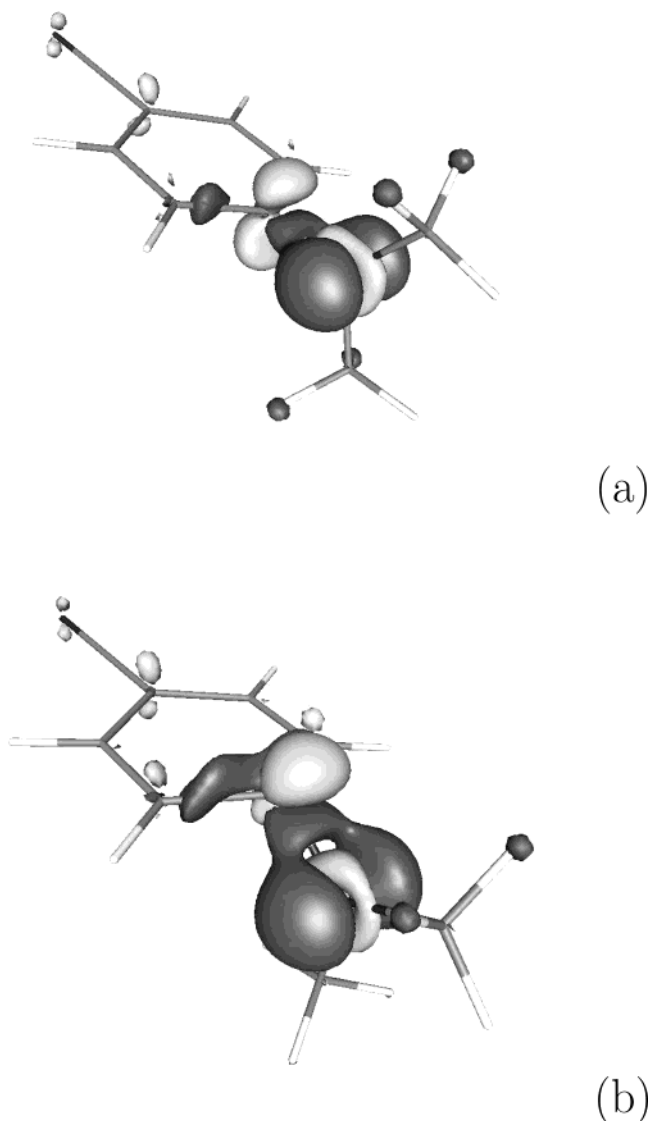


Figure 5. Difference density (ICT state density minus ground-state density) (a) at the C_{2v} symmetric minimum structure and (b) at the C_s symmetric minimum structure. See also Figure 3 for explanations.

C_{2v} and the C_s structure occur. It is not possible, however, to decide, based on these differences, which of both structures is closer to the experimental one.

The predicted ring stretching modes reveal a stronger quinoid character of the ring bonds than in the ground state. This is also obvious from the C–C force constants in Table 3 which indicate a very strong central carbon–carbon bond. This gives rise to two modes, 8a and a mixture of 14 and 19b, at 1617 cm^{-1} and 1533 cm^{-1} which have nearly exclusive C_2 – C_3 double bond stretching character. Only the a_1 symmetric linear combination of the two double bond stretches, 8a, is clearly observable in the Raman spectrum,²⁹ but the resolution of the spectrum is not high enough to exclude the presence of a presumably weaker band corresponding to the b_2 symmetric mode. Further ring stretching modes that can be assigned to experimental bands are as follows: the ring breathing mode 1 at 746 cm^{-1} , experimentally observed at 756 cm^{-1} and again with contributions from 6a bending, and 12 bending mixed with 19a stretching at 949 cm^{-1} which is experimentally found at 984 cm^{-1} (ref 29) and 959 cm^{-1} (ref 30). The band calculated

at 1326 cm^{-1} , another linear combination of 19b and 14, may correspond to the nontotally symmetric part of the band at 1276 cm^{-1} reported in ref 30. Above that, ring stretching modes contribute significantly to other normal modes. In particular the 18a-like hydrogen in-plane bending mode calculated at 1430 cm^{-1} has contributions from 19a and may be assigned to the band found at 1425 cm^{-1} in time-resolved IR spectra.^{30,31} This band is not observed in the Raman experiments;²⁹ rather a band at 1358 cm^{-1} is reported which we may ascribe to another hydrogen in-plane bending mode (see Table 5).

The normal mode calculated at 1219 cm^{-1} involves predominantly a stretch of the phenyl–cyano bond; the experimental fundamental lies at 1220 cm^{-1} . Both calculation and experiment agree that, as compared to the ground state, this band is only slightly shifted towards lower frequencies by -17 cm^{-1} and -7 cm^{-1} , respectively. The force constant associated with that bond even rises (see Table 3). In contrast to that, the vibration calculated at 1290 cm^{-1} which is mainly a phenyl–nitrogen stretch, is predicted to shift down by -100 cm^{-1} . Experimentally this band is found at 1276 cm^{-1} , corresponding to a downshift of -96 cm^{-1} . The force constant of the Ph–N bond has now a value that indeed corresponds to a single bond. Likewise, the stretching mode of the cyano group is strongly red-shifted. CC2 predicts this band at 2030 cm^{-1} resulting in a shift of -74 cm^{-1} compared to the ground state. Experimentally, a shift of -109 cm^{-1} is found in aprotic solvents such as acetonitrile,⁵⁹ while a larger shift is observed in protic solvents, e.g., -124 cm^{-1} in methanol.^{29,59} Recently, Kwok et al.⁵⁹ put forward evidence indicating that this stronger shift is due to hydrogen bonding.

3.5. Reliability of the Calculations: Comparison to High-Level Coupled-Cluster Calculations. Before discussing the implications of the presented results, we shortly address the reliability of the method employed. First of all, we have implemented some diagnostic criteria (for details, see refs 38 and 39) which allow (at low computational expense) monitoring the potential multireference character of the ground state and the amount of double excitation contributions to the excitation. These criteria indicate that at all ground and excited state geometries the ground state wave function is sufficiently well described by a single reference.⁶⁹ The excited states, however, have a sizeable double excitation contribution. Therefore some tests with higher-level coupled-cluster methods appeared necessary.

We focus on three issues: (a) The pyramidalization of the ICT state, (b) the relative energy of the LE and the ICT state, and (c) the adiabatic excitation energy for the LE state. We carried out single-point CCSD and CCSDR(3) calculations (using the CC2/TZVPP structures) as well as CASSCF calculations (including geometry optimizations at that level) using a smaller basis set (as described in section 2).

The energy differences between a C_{2v} -symmetric TICT structure (1^1A_2 state) and the pyramidalized C_s ($1^1A''$ state) structure obtained at these levels of theory are listed in the last column of Table 6. The CCSD and CCSDR(3) calculations confirm the CC2 results, where CC2 fortuitously lies closer at the triples-corrected CCSDR(3) result than CCSD does. As coupled-cluster methods, in the case of a larger double-excitation contribution to an excited state, may be biased towards the

(69) In ref 26, it was noted, however, that, for twisted geometries, the Hartree–Fock solution becomes triplet-unstable.

Table 5. Calculated (CC2/TZVPP) Harmonic Frequencies and Isotopic Shifts for Selected Modes of the ICT State of DMABN in Comparison to Experimental Observations (the Modes Are Designated According to the Point Group C_{2v} ; for the Definition of the Isotopomers, See Text)

mode	DMABN		DMABN- ^{15}N		DMABN- d_6		DMABN- d_2		assignment
	ν_{ca}^a	ν_{ob}^b	$\Delta\nu_{ca}^c$	$\Delta\nu_{ob}^d$	$\Delta\nu_{ca}^c$	$\Delta\nu_{ob}^d$	$\Delta\nu_{ca}^c$	$\Delta\nu_{ob}^d$	
4 a ₁	746, 757	756 ^e	0	-1 ^e	-10	-9 ^e	-18		1,6a
5 a ₁	887, 899	907 ^e	-7	-4 ^e	-100	-106 ^e	+9		ν_{N-Me}^s
6 a ₁	949, 965	984 ^e , 959 ^f	0	+3 ^e , +1 ^f	0	+1 ^e , +0 ^f	-131	-8 ^f	12, 19a
7 a ₁	1123, 1056	1116 ^e	0	-1 ^e	-108	-99 ^e	+13		ρ_{Me} , ν_{Ph-N}
9 b ₂	1148, 1228		-3		-10		-5		8b
8 a ₁	1181, 1183	1170 ^e	0	0 ^e	-2	-4 ^e	-160		δ_{C-H}
9 a ₁	1219, 1224	1221 ^e , 1220 ^f	0	0 ^e , 0 ^f	-5	-9 ^e , -2 ^f	-18		ν_{Ph-CN} , 1, 12
10 a ₁	1290, 1274	1281 ^e , 1276 ^f	-17	-20 ^e , +4 ^f	-44	-32 ^e , -27 ^f	-1	+1 ^f	ν_{Ph-N} , ρ_{Me}
10 b ₂	1326, 1317	1276 ^{g,f,h}	0	$\sim +4^f$	+1	-2 ^f	-5		19b, δ_{C-H} , 14
11 b ₂	1340, 1389	1358 ^e	0	-6 ^e	0	0 ^e	-86		δ_{C-H}
12 a ₁	1430, 1433	1425 ^f	0	+1 ^f	0	+1 ^f	-54	-55 ^f	δ_{C-H}
13 a ₁	1490, 1484	1502 ^e	-1	+2 ^e	-373	-8 ^e	0		δ_{Me}
13 b ₂	1533, 1545		0		0		-9		14, 19b
14 a ₁	1617, 1604	1580 ^e	0	-2 ^e	0	+1 ^e	-9		8a
15 a ₁	2030, 2043	2095 ^e , 2091 ⁱ , 2104 ^j	0	0 ^e	0	0 ^e	-1		ν_{CN}

^a Calculated harmonic frequency in cm^{-1} . Results for the C_{2v} (first value in column) and the C_s structure (second value) are given (see text). ^b Observed fundamental band in cm^{-1} . ^c Calculated frequency shift in cm^{-1} . For better legibility, only those for the C_{2v} structure are given. ^d Observed frequency shift in cm^{-1} . ^e Time-resolved resonance Raman in methanol with 330 nm probe (from ref 29) ^f Time-resolved IR in acetonitrile (from refs 30 and 31). A star indicates experimental evidence for a nontotally symmetric character of the vibrational mode. ^g Band vanishes on substitution. ^h Antisymmetric band overlapping with 10 a₁. ⁱ Time-resolved IR in methanol from ref 59. ^j Time-resolved IR in acetonitrile from ref 59.

Table 6. Comparison of the Predictions of Several Theoretical Models for the Adiabatic Excitation Energy between Ground State and LE State, $T_e(\text{LE})$, the $\text{LE} \rightarrow \text{ICT}(C_{2v})$ Reaction Energy and the Relaxation Energy of the ICT State upon Assuming the Distorted C_s Structure

	$T_e(\text{LE})$	ΔT_e	
		[$\text{LE} \rightarrow \text{ICT}(C_{2v})$]	[$\text{ICT}(C_{2v}) \rightarrow \text{ICT}(C_s)$]
CC2/TZVPP	4.142	+0.014	-0.081
CC2/SVP ^a	4.283	-0.070	-0.103
CCSD/SVP ^a	4.497	+0.129	-0.081
CCSDR(3)/SVP ^a	4.322	+0.160	-0.100, -0.094 ^b
CASSCF/SVP			-0.027 ^c , -0.031 ^d , -0.057 ^e

^a Using CC2/TZVPP structures. ^b Using CASSCF(12e/11o)/SVP structures. ^c Active space (6e/5o). ^d Active space (10e/9o). ^e Active space (12e/11o).

ground state, we also carried out CASSCF calculations. We found for all tested active spaces that again the pyramidalized form is energetically more favorable.⁷⁰ The stabilization energy increases with the size of the active space.

The bond distances in the cyano group do not seem to be an issue, either, as CCSDR(3) calculations at the CC2 and the CASSCF geometries (where the cyano-bond is significantly shorter) have nearly identical results. To summarize, we can conclude that CC2 describes the ICT state correctly.

At the CC2/TZVPP level, the energy difference between the LE state and the C_{2v} symmetric ICT state is predicted to be very small, the ICT state lying higher in energy by 0.014 eV. Including the energy lowering of this state through pyramidalization, however, this results in an ICT state which is by 0.08 eV lower than the LE state; i.e., an exotherm $\text{LE} \rightarrow \text{ICT}(C_s)$ reaction is predicted. This picture changes if we include the full double-excitations (CCSD) and triples corrections (CCSDR(3)) (see Table 6). There is also a notable basis set effect as can be seen from the CC2 results for SVP and TZVPP.

(70) This is in contradiction to what was reported in ref 21. The authors claim to have located a C_{2v} -symmetric minimum for the TICT state. From the absolute energy given in the supplement to their article, we conclude that state-averaging was used which may explain the different result. State-averaging, however, is problematic for the ICT state, since the active space is too small to account for the large relaxation effects upon transition from the ground state to the ICT state.

We take the difference between the CC2/SVP and the CCSDR(3)/SVP results to correct the CC2/TZVPP results for higher-order effects. Including also the zero-point energy from the CC2/TZVPP harmonic force fields, we obtain our best estimate for the $\text{LE} \rightarrow \text{ICT}(C_s)$ interconversion which is now predicted to be endothermic by 0.17 eV (16 kJ mol⁻¹).

The adiabatic excitation energy of the LE state again lies at the CC2 level (somewhat fortuitously) closer to the CCSDR(3) result than the CCSD result does. Our best estimate for ν_{00} of this state thus corrects the CC2/TZVPP value (cf. section 3.3) only slightly towards higher energy resulting in 4.001 eV, which even better compares with the experimental value of 3.998 eV.^{53,55} Note, however, that the expected accuracy of the extrapolated value should only be on the order of ± 0.2 eV.

4. Implications on the ICT Mechanism

According to our calculations, mainly three coordinates contribute to the reaction path of the $\text{LE} \rightarrow \text{ICT}$ reaction: (a) the twisting motion of the dimethyl-amino group, (b) the pyramidalization of the ring carbon atom to which the dimethyl-amino group is attached, and (c) the quinoidization modes (8a and 8b) of the ring moiety, as the molecule transforms from an anti-quinoid LE state into a quinoid ICT state.⁷¹ We may be tempted to conjecture that coordinate a and a proper linear combination of coordinates b and c make up the branching space of the conical intersection between the LE and the ICT state. However, a more thorough analysis of the PES near the conical intersection is demandable for definitive conclusions.

For the gas-phase reaction, CC2 predicts the LE and ICT states to have about the same energy, and a barrier on the order of 0.1 eV may be estimated from the available calculated data. Comparison with higher-order coupled-cluster expansions (sec-

(71) Zilberg and Haas (ref 24) also discuss quinoid and anti-quinoid minima and the significance of the quinoidization modes on the excited-state surface of *p*-pyrrolobenzonitrile. Based on their CASSCF calculations, they suggest that a quinoid ring structure is connected with a PICT-like minimum whilst the TICT-like minimum has an anti-quinoid ring structure. We have to note, however, that the claimed TICT minimum is an A₁ state in that study, whereas an A₂ state would be expected to be the direct counterpart of the TICT state in DMABN.

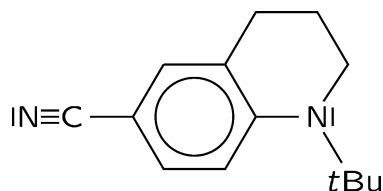


Figure 6. Structural formula of 1-*tert*-butyl-6-cyano-1,2,3,4-tetrahydroquinoline (NTC6).

tion 3.5), however, indicates that the LE \rightarrow ICT reaction may be endothermic by up to 0.17 eV. In previous theoretical work, values of 0.3 eV (using a coupled-cluster variant and ground state geometries¹⁹) and between -0.04 eV and -0.4 eV (using CASPT2 and DFT/MRCI based on semiempirical or CIS excited state geometries²⁰) have been put forward. Unfortunately, the attainable accuracy in the theoretical treatment of excited states in molecular systems of the current size is still limited and our best estimate for the energy difference may still be in error by around 0.2 eV. Indeed, experimental observations^{55,67,68} seem to indicate a barrier around 0.1 eV and a LE \rightarrow ICT reaction energy well below that value.

Trushin et al.⁶⁸ have recently observed coherent oscillations in the femtosecond time-resolved photoionization spectrum of DMABN which were attributed to low-frequency oscillations of the molecule in the LE well. They were assigned to the amino group twist and inversion (or “wagging”) modes, and the conical intersection was assumed to be displaced along these coordinates. We note however, that the assignment of these low-frequency modes based on quantum chemical calculation require a very accurate treatment including anharmonicity effects, which is so far not available. We only remark that in our calculations the conical intersection is displaced along the coordinates described in the first paragraph of this section and that we therefore expect that these modes will trigger the observed oscillations.

As we did not consider solvent effects in our calculations, of course no direct comparison with experiments in solution is possible. Yet we find that we can very consistently assign large parts of the experimental IR and Raman spectra, which indicates that the intermediates involved in the ICT reaction in solution do not significantly differ from those in the gas-phase. Although this interpretation has to be taken with caution because of the presence of strong mixing with other modes, it constitutes, supported by the present theoretical data, clearly an argument in favor of the TICT mechanism.

The assumptions of the PICT model, in particular a planar ICT state, are clearly not supported by the current calculations, as on the ICT hypersurface no stationary point with a PICT-like structure can be localized (see section 3.2). Nevertheless, the energy gap considerations put forward by Zachariasse et al.^{6,9} are certainly a second important ingredient for the prediction of dual fluorescence.²⁵ They are, however, independent of the actual ICT mechanism.

Yet, as mentioned in the Introduction, very recently experimental evidence was put forward which was interpreted as an obvious contradiction to the TICT hypothesis:¹³ Efficient ICT was observed for NTC6, Figure 6, a molecule which hitherto has been considered as planarized, as the amino group is part of a six-ring sharing two carbon atoms with the aromatic benzonitrile moiety. It was therefore concluded that the formation of a twisted ICT state is not possible and that another

mechanism must be responsible for the observed highly polar state. Our calculations on DMABN, however, indicate that in the excited state the phenyl-ring is more flexible than in the ground state. In particular, the aromatic carbon-atom adjacent to the nitrogen-atom turns into a more or less sp^3 hybridized center (see Figure 5b) allowing for a conformation of the aliphatic six-ring of NTC6 in which a nearly planarized amino group may readily be twisted, relative to the benzonitrile moiety. The conclusion is that the data presented in ref 13 do not necessarily exclude a TICT mechanism. Computational efforts to substantiate this conjecture are under way.

Finally, we want to give a short remark concerning the “electronic decoupling” or “principle of minimum overlap”, respectively.⁴ We have carried out calculations for the triplet excited states too and found that at $\tau = 90^\circ$ both singlet and triplet state have a nearly identical structure and, within 0.01 eV, the same energy. This indicates that indeed the exchange interaction of the particle-hole pair vanishes and, in this sense, one can speak of electronic decoupling between the two moieties. The triplet states of DMABN will be further examined in a forthcoming publication.

5. Summary

We have presented a pure ab initio treatment of the ground state and the two fluorescing states of DMABN, which involved the full treatment of valence electron correlation using the CC2 model in combination with large triple- ζ basis sets and full geometry optimizations. To the authors’ best knowledge, this is also the first study on the vibrational spectra of the excited states of DMABN using a correlated method.

The present study supports the TICT hypothesis in the sense that the twisting of the dimethyl-amino group clearly is the dominant reaction coordinate that leads from the locally excited state to a low-lying ICT state. On the other hand no indication for a PICT-like stationary point on the potential energy hypersurface was found. We want to emphasize, however, that the capability of a molecule to form a TICT state is only a necessary but not a sufficient condition to predict the phenomenon of dual fluorescence. More elaborate criteria for such a prediction have been recently put forward by Jamorski and Lüthi.²⁵

Further active coordinates that are involved in the LE \rightarrow ICT reaction are the quinoidization modes and an out-of-plane mode that involves the carbanion-like pyramidalization of the ring carbon atom adjacent to the dimethyl-amino group. The latter coordinate has so far not been considered in studies of that molecule. In our calculations, however, we find that the C_{2v} symmetric TICT state is only a saddle point with respect to this coordinate and the relaxed structure is predicted to possess C_s symmetry. This result is confirmed by CASSCF optimizations and single-point CCSDR(3) calculations based on both CC2 and CASSCF geometries. The additional structural flexibility introduced by this degree of freedom may be of substantial importance for the explanation of ICT in so-called “planarized” molecules such as NTC6, where the aminogroup is fixed to the benzene ring by a $(CH_2)_n$ bridge.

The LE \rightarrow ICT gas-phase reaction is predicted to be slightly exothermic by 0.07 eV (7 kJ mol⁻¹) at the CC2/TZVPP level; including higher-order corrections from a CCSDR(3)/SVP calculation, we find the reaction to be endothermic by 0.17 eV (16 kJ mol⁻¹).

The vibrational spectra of solvated molecules recorded for both ground and excited states can be consistently interpreted on grounds of vibrational frequencies deduced from the CC2 harmonic force field. We can confirm that the observed band shifts, especially for the Ph–N stretching mode, may be *qualitatively* correlated with the force constants of these bonds. But we have to add that the Ph–N stretching mode lies in a frequency region where many other modes are present to which it can couple strongly, thus making an a priori correlation between frequency and bond strength difficult, if not impossible. In connection with the theoretical data from this paper and the preceding TDDFT study,²⁶ however, the downshift of the Ph–N mode in the ICT state, as found in recent time-resolved Raman experiments, can be taken as an indication for the presence of a TICT-like structure in solution.

With respect to TDDFT as a tool to investigate ICT states, we have to give two comments: First of all we do not want to conceal that in terms of computation time TDDFT is by far more efficient than CC2, surely allowing to investigate molecules of much larger size than DMABN. But it must be added, as our second comment, that currently available functionals do not satisfactorily reproduce the energetics of ICT processes. This applies not only to the adiabatic excitation energy of the ICT state itself which is found to be more than 0.5 eV too low with TDDFT²⁶ but also to the LE state, for which an erroneous nearly constant minimum path along the torsion coordinate is predicted.²⁶ On the other hand, as long as these effects do not completely spoil the local potential hypersurface, TDDFT can quite well provide vibrational normal modes and dipole mo-

ments of the excited states. This gives perspective to the treatment of large ICT systems, provided that density functional development succeeds to solve the above-mentioned problems.

We may finally add that there are many aspects of the dual fluorescence phenomenon which are associated with solvent effects (simply as most experiments are carried out in solution phase), and it is worthwhile to be able to include them in future theoretical work. Steps in this direction have already been undertaken using either continuum models²³ or molecular-dynamics simulations,¹⁷ but clearly improved solvation models and a combination with more reliable methods to obtain excited state geometries are desirable. With respect to the latter, CC2 excited state gradients certainly are a contribution.

Acknowledgment. This work was supported by the Center for Functional Nanostructures (CFN) of the Deutsche Forschungsgemeinschaft (DFG) within Project C2.1; further support within DFG Project HA 2588/2-1 is gratefully acknowledged as well. The authors want to thank D. Rappoport and Dr. F. Furche for many fruitful discussions. We are also indebted to Dr. F. Weigend for providing us with a preliminary version of his computer routines to generate density plots.

Supporting Information Available: Cartesian coordinates of all RI-CC2/TZVPP structures considered in this paper (ASCII text). This material is available free of charge via the Internet at <http://pubs.acs.org>.

JA0490572